

Cite this article as: Li Kun, Wen Tengfei, Li Shaolong, et al. Effects of Ultrasonic Shot Peening on Surface Integrity and Corrosion Resistance of 6061-T6 Aluminum Alloy[J]. Rare Metal Materials and Engineering, 2025, 54(07): 1717-1726. DOI: <https://doi.org/10.12442/j.issn.1002-185X.20240334>.

ARTICLE

Effects of Ultrasonic Shot Peening on Surface Integrity and Corrosion Resistance of 6061-T6 Aluminum Alloy

Li Kun, Wen Tengfei, Li Shaolong, Wang Cheng

School of Mechatronics Engineering, Anhui University of Science & Technology, Huainan 232001, China

Abstract: According to surface morphology, microhardness, X-ray diffraction, and static contact angle experiments, the changes in the surface integrity and corrosion resistance of 6061-T6 aluminum alloy after ultrasonic shot peening (USP) were investigated. Results show that the grain size of the material surface is reduced by 43%, the residual compressive stress has an increasing trend, the roughness and hardness are increased by approximately 211.1% and 35%, respectively. And the static contact angle is increased at first, followed by a slight decrease. Weighing, scanning electron microscope, and energy dispersive spectrometer were used to study the samples after a cyclic corrosion test. Results show that USP reduces the corrosion rate by 41.2%. A model of surface corrosion mechanism of USP is developed, and the mechanism of USP to improve the corrosion resistance of materials is discussed. The introduction of compressive residual stresses, grain refinement, increased grain boundaries, increased hardness, and increased static contact angle are the main factors related to the improvement of corrosion resistance in most materials, while increased roughness tends to weaken surface corrosion resistance.

Key words: 6061-T6 aluminum alloy; corrosion resistance; surface integrity; USP

1 Introduction

The 6061 aluminum alloy (Al-Mg-Si) is a typical precipitation-hardening aluminum alloy. The addition of Mg, Si, and other elements makes the alloy lightweight and corrosion-resistant, with high specific strength and easy to process. Therefore, the 6061 alloy performs excellently in a wide range of applications, including railway vehicles, ships, aerospace, and other industrial fields^[1-3]. However, with the growing demand for 6061 aluminum alloy, particularly for marine applications, the surface of material may be susceptible to a range of corrosion-related damages, such as pitting corrosion, stress corrosion cracking, and intracrystalline corrosion, which can affect its mechanical properties^[4-7]. Strengthening metal surfaces improves corrosion resistance and extends the service life of the material^[8], which can be done through a variety of techniques, such as laser shock peening^[9-10], ultrasonic impact treatment^[11], and ultrasonic shot peening (USP)^[12-13].

USP is a simple and efficient material surface strengthening process. It uses ultrasonic vibration as a source of energy to drive high-speed impacts of shots on the surface of the material to strengthen it, as well as improve its corrosion resistance^[14-16], fatigue resistance^[17], and wear resistance^[18]. USP is widely used in such applications, owing to its range of advantages regarding high accuracy, easy control of experimental conditions, small size, and low working energy consumption^[19]. Material surface integrity represents an important factor related to corrosion behavior in terms of properties, such as roughness, hardness, residual compressive stress, and others. Zhang et al^[20] performed USP of titanium matrix composites at various durations and found that the compressive residual stress field increased with the increase in shot peening duration, and the maximum microhardness increased by 48% after USP. Ganguly et al^[21] reduced the corrosion rate of AZ91 magnesium alloy by adding graphene nanosheets, further reduced the corrosion rate after USP, and finally concluded that the best corrosion resistance was

Received date: July 04, 2024

Foundation item: Introduction of Talent Research Start-up Fund of Anhui University of Science and Technology (2022yjrc35); Colleges and Universities Excellent Young Talents Domestic Visit Research Project of Anhui Province (gxgnfx2022006)

Corresponding author: Li Kun, Ph. D., Associate Professor, School of Mechatronics Engineering, Anhui University of Science & Technology, Huainan 232001, P. R. China, E-mail: kli@aust.edu.cn

Copyright © 2025, Northwest Institute for Nonferrous Metal Research. Published by Science Press. All rights reserved.

achieved by adding 2.0wt% of graphene nanosheets following USP technique for 20 s. Liu et al.^[15] treated an AA7034 aluminum alloy via USP technique, polishing, and both methods. They reported that the corrosion rate increased in the samples only treated by USP, but decreased in the samples treated by both USP and polishing. Kumar et al.^[22] showed that excessively long USP durations can cause localized damage to the material surface, which counteracts the beneficial effects of surface grain refinement and residual compressive stresses, thus reducing corrosion resistance of the material. Therefore, inappropriately using USP, which increases the surface roughness of the material, negatively impacts its corrosion resistance. It is crucial to note that the selection of inappropriate USP parameters may weaken the corrosion resistance of a treated material.

These studies have shown that treatment with appropriate USP process parameters has a positive impact on improving material properties. However, there are fewer studies regarding the mechanism underlying the corrosion resistance conferred by USP on 6061-T6 aluminum alloy. This study was conducted to strengthen the surface of this material through varying durations of USP treatment, and characterize its surface integrity. The effect of USP duration on the cyclic corrosion performance of this alloy was also evaluated to clarify the optimal treatment parameters. The results of this study will promote the further application of 6061 aluminum alloy in corrosive marine environments.

2 Experiment

The 6061-T6 aluminum alloy used in this test is a high-quality aluminum alloy produced via the heat-treatment and pre-stretching process. Its chemical composition is shown in Table 1, and the size of sample used for our tests is 80 mm×15 mm×2 mm. The surface of each sample was polished with sandpaper, to minimize surface scratches. The polished samples were then cleaned with anhydrous ethanol and dried for the treatments.

Our experiments used self-designed USP equipment, consisting of an ultrasonic generator, ultrasonic vibration system, and shot peening chamber. The selected USP system was model DW-KZB15-2600S, with a power of 2600 W and a shot peening chamber measuring 71 mm in diameter. The ultrasonic generator converts electrical current into a 15 kHz ultrasonic vibration signal. USP system converts this ultrasonic vibration signals into physical ultrasonic vibrations, which stimulates the movement of the shots in the shot peening chamber, allowing for surface strengthening of the samples through shot peening. The shot material was zirconium oxide ceramic. In this study, the shots covered the bottom of the shot peening chamber with a layer to determine the number of shots.

Table 1 Chemical composition of 6061-T6 alloy (wt%)

Si	Mg	Cr	Cu	Mn	Zn	Ti	Fe	Al
0.4–0.8	0.8–1.2	0.04–0.35	0.15–0.40	0.15	0.25	0.15	0.7	Bal.

The various USP parameters used in this study are shown in Table 2. The effect of shot peening durations on the surface integrity of 6061-T6 aluminum alloy was investigated in samples T1–T5. Electrical spark wire cutting was performed on the original samples, as well as on those treated by USP, and the area covered by the shot peening was cut down to a size of 30 mm×15 mm×2 mm for subsequent experiments.

A microhardness tester (HV-1000Z, SCTMC, China) was used to measure the Vickers microhardness of the original and treated samples, using a loading force of 0.49 N, a holding duration of 10 s, and a multiplication rate of 40. To minimize errors, measurements were taken for 10 randomly-selected positions on the surface of each sample, and the average of these 10 measurements was taken to represent the Vickers surface hardness value of material.

Both treated and untreated (UT) samples were scanned using a non-contact 3D profilometer (PS50, NANOVEA, USA), with a scanning step size of 6 μm and a waveform capture rate of 400 Hz. Two-dimensional (2D) and three-dimensional (3D) surface topographies and roughness parameters, including arithmetic mean deviation (R_a), root-mean-square deviation (R_q), and total height of the contour (R_z), were obtained for each of the six sample groups. As the roughness measurements varied significantly for different points on the observation area, the roughness values of 20 points were taken for the average value, to reduce error and to better analyze the effects of different USP treatment durations on surface roughness.

The section to be observed was cut from each sample and mounted. It was polished with metallographic sandpaper to 2000#, then with diamond grinding paste in a polishing machine. The samples were etched with Keller's reagent for 3 min to observe their microstructures, then cleaned with anhydrous ethanol and dried. Their microstructures were observed using an optical microscope (OM, GX51, OLYMPUS, Japan). The surface morphology of each sample after corrosion was analyzed using a scanning electron microscope (SEM, FlexSEM1000, HITACHI, Japan), and compositional changes in each sample before and after corrosion were analyzed using an energy dispersive spectrometer (EDS, 550i, IXRF, USA) coupled to SEM.

The phase and compressive residual stresses distribution of all samples were determined using X-ray diffractometer (XRD, SmartLab, Rigaku, Japan), using a Cu-Kα radiation source with an output power of 3 kW, a scanning speed of

Table 2 Experimental process parameters

Sample	USP duration/s	Shot diameter/mm	Peening distance/mm
T1	50	4	60
T2	100	4	60
T3	200	4	60
T4	300	4	60
T5	400	4	60
UT	/	/	/

5°/min, and a scanning range (2θ) of 5°–90°. The test data were processed by Jade software to analyze the variation in grain size and the surface phase composition of each sample.

Static contact angle measurements for the untreated sample and five groups of treated samples were conducted via the seated drop method, using a contact angle measuring instrument (DSAeco Plus, KRÜSS, Germany). The contact medium was a 5wt% sodium chloride (NaCl) solution with a volume of 3 μL. Contact angles were measured at three random points for each sample, and the average value was taken to represent the static contact angle for that sample.

According to Chinese national standards, using a neutral salt spray environment to simulate a marine corrosive environment^[23], the experiments were conducted in a salt spray chamber (cct2s, SUGA, Japan) with the surface of the material oriented vertically at 20°. Every experiment alternated between a salt spray condition for 2 h, a dry condition for 4 h, and a wet condition for 2 h. These cyclic experiments were conducted 36 times. The schematic diagram of cyclic corrosion test (CCT) environmental spectrum is shown in Fig.1. The samples were immersed in concentrated nitric acid (ρ=1.42 g·mL⁻¹) for 4 min after completion of the corrosion experiment, then cleaned using anhydrous ethanol and dried. Finally, each sample was weighed (to the nearest 0.1 mg), and the corrosion rate could be calculated using Eq.(1)^[24]:

$$V = \frac{(m_0 - m) \times 8.76 \times 10^4}{AtD} \quad (1)$$

where *V* is the corrosion rate (mm·a⁻¹), *m*₀ is the mass of the sample before corrosion (g), *m* is the mass of the corrosion

product after corrosion (g), *A* is the area of the corrosion surface (4.5 cm²), *t* is the corrosion time (288 h), and *D* is the density of the sample (2.7 g·cm⁻³).

3 Results

3.1 Microstructure

After USP treatment, the formation of dense dislocations, deformation twins, and grain refinement in the samples was promoted by the combination of high strain rate plastic deformation and compressive residual stresses^[25]. Fig.2 shows the microstructures of 6061-T6 aluminum alloy surfaces before and after USP treatment. Fig.2a₁, Fig.2a₂, Fig.2b₁, and Fig.2b₂ are enlarged drawing of the selected areas in Fig.2a and Fig.2b with a magnification of 15. It can be seen that the grain size of the sample's surface layer after USP treatment was reduced, its grain boundaries increased, and the grain refinement effect was significant. Looking inward along the USP-treated surface of the material, the grain size gradually transitioned to the base material microstructure.

The grain size of the original sample and that after different durations of USP treatment were analyzed using the truncated line method. Three measurements were taken for each sample's surface and the average value was taken as the average surface grain size. The average grain size can be expressed by Eq.(2):

$$a = \frac{l}{n} \quad (2)$$

where *a* is the average grain size of the sample (μm), *l* is the length of the straight line taken in the microstructural metallographs (μm), and *n* is the total number of grains intercepted by the straight line. The results are shown in Table 3. A significant negative correlation was found between the surface grain size and the treatment duration. A comparison of UT and T1 samples showed that the grain size of surface layer was significantly reduced after USP treatment. A comparison of T1–T5 samples revealed that the surface grain size decreased gradually with the increase in USP duration. The surface grain size of the sample treated for 400 s reached a minimum value of 15.41 μm, which was 42.9% lower than that of the UT sample.

3.2 XRD analysis

Fig. 3 presents XRD patterns of samples under different

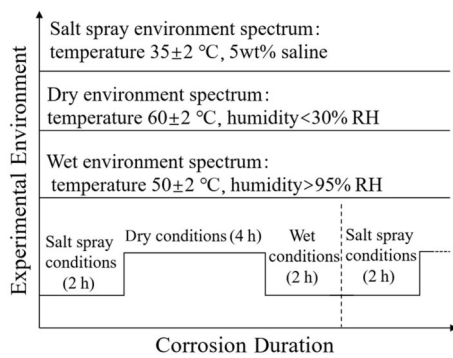


Fig.1 Schematic diagram of CCT environmental spectrum

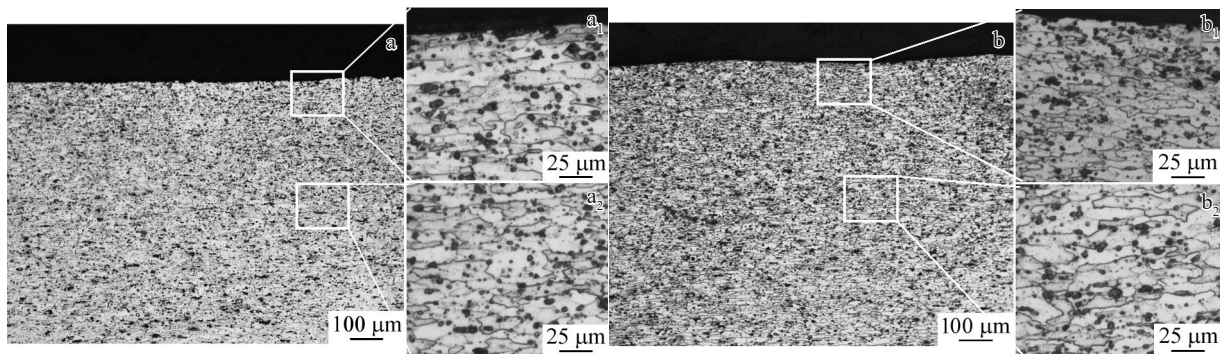
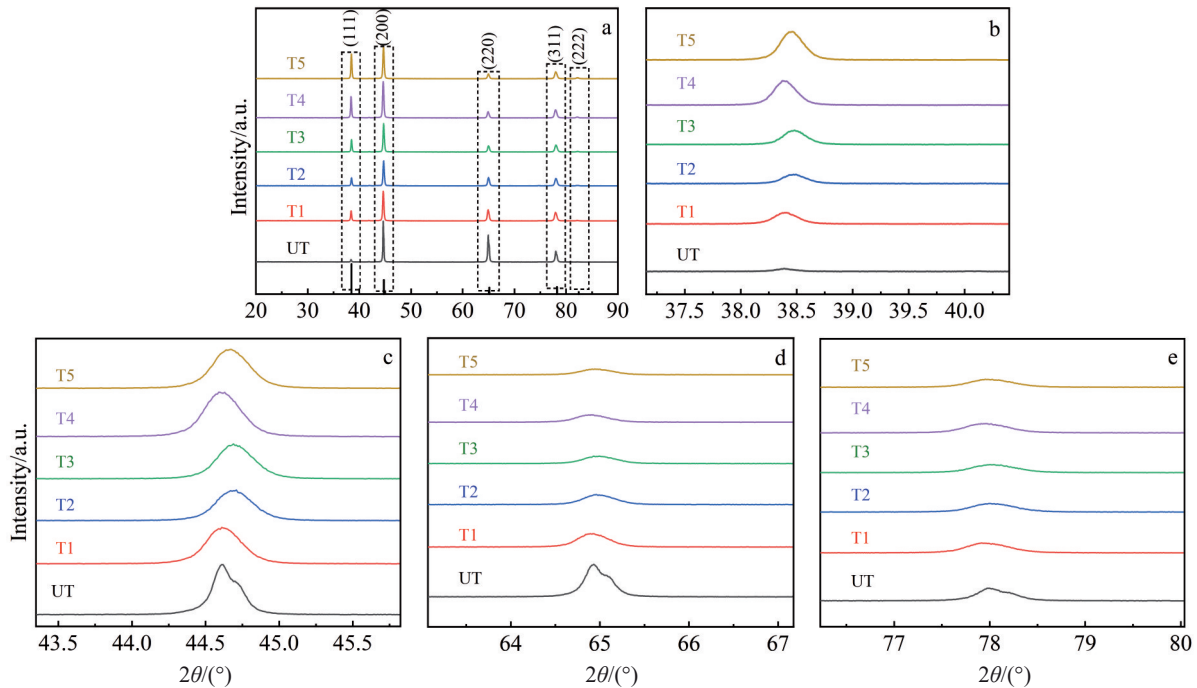


Fig.2 Cross-sectional microstructural metallographs of UT sample (a) and T2 sample (b)

Table 3 Surface grain sizes of samples treated by USP with different durations

Sample	USP duration/s	First measurement/ μm	Second measurement/ μm	Third measurement/ μm	Average value/ μm
UT	0	26.76	27.49	26.73	26.99
T1	50	17.71	18.37	17.94	18.06
T2	100	17.54	16.65	17.65	17.28
T3	200	16.12	16.27	15.94	16.22
T4	300	15.83	15.70	16.02	15.85
T5	400	15.75	14.93	15.54	15.41

**Fig.3** XRD patterns of all samples (a), enlarged XRD patterns of peaks (111) (b), (200) (c), (220) (d), and (311) (e)

USP durations. Five diffraction peaks of α -Al are found in Fig.3a, including peaks (111), (200), (220), (311), and (222). It can be seen in Fig. 3 that no new diffraction peaks are produced, indicating that USP treatment does not cause the material to produce new phases. The two major factors influencing the shift of the diffraction peaks are the composition of the solid solution and the residual stress state. The introduction of compressive residual stress shifts the diffraction peak to the right. The dissolution of the secondary phase shifts XRD diffraction peak to the left^[26]. All diffraction peaks of T1 – T5 samples were shifted to the right with different degrees compared to the UT sample (Fig. 3b–3e), which indicates that the compressive residual stresses have a greater effect on XRD diffraction peak displacement than the secondary phase dissolution. And the residual compressive stresses of the samples were all increased after USP treatment. From Fig.3 and Table 4, it can be seen that full width at half maximum (FWHM) values of all diffraction peaks of T1–T5 samples were increased compared to UT sample, which is mostly attributed to grain refinement and severe lattice deformation^[27].

Table 4 FWHM of samples treated by USP with different durations

Lattice plane	UT	T1	T2	T3	T4	T5
(111)	0.188	0.212	0.225	0.231	0.235	0.238
(200)	0.198	0.268	0.274	0.281	0.287	0.290
(220)	0.296	0.360	0.373	0.388	0.394	0.401
(311)	0.382	0.468	0.479	0.487	0.495	0.503

3.3 Surface Vickers hardness

The measured hardness values of the samples are shown in Fig. 4. The initial surface hardness of UT sample was 108.1 HV, which was enhanced after USP treatment. The increment of hardness values with the increase in peening duration were 18.7, 25.0, 33.9, 37.8, and 37.3 HV. The surface hardness of the sample treated for 300 s reached a maximum value, which was 35% higher than that of the UT sample. The surface hardness of the sample treated for 400 s did not increase any further. This indicated that the surface hardness had reached its maximum value after USP treatment for 300 s. Taken together with the analysis presented in Fig. 4, the surface

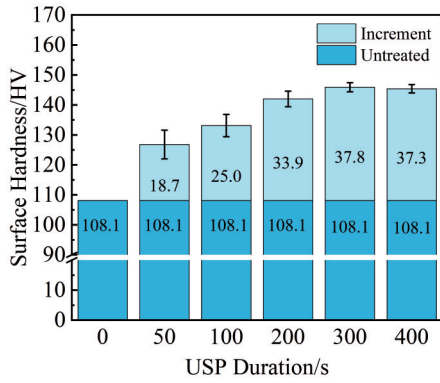


Fig.4 Effect of USP duration on surface hardness of samples

hardness of USP-treated samples increased significantly compared to the untreated samples. The surface hardness of the samples gradually increased with the increase in USP duration, but the average hardness growth rate gradually decreased after 300 s. The final surface hardness tended to stabilize after this point.

After USP treatment, grain refinement and increased grain boundaries occurred on the surface layer of material. The strength of the 6061-T6 aluminum alloy changed after grain refinement, following the Hall-Petch relationship^[28]:

$$\sigma_y = \sigma_0 + \frac{k_y}{\sqrt{d}} \quad (3)$$

where σ_y is the yield limit of the material (MPa), d is the grain size (μm), σ_0 is the lattice frictional resistance that occurs

when moving a single dislocation, and k_y is a constant. According to the Hall-Petch relationship, a decrease in grain size (d) increases the yield limit (σ_y) of the material. Moreover, USP treatment introduces a high density of dislocations in the surface layer of the material, which exerts a work-hardening effect. As a result, the surface hardness of each USP-treated sample increased significantly through various strengthening effects, such as fine grain strengthening and work hardening^[29]. Past a certain treatment duration, the fine grain strengthening effect is also enhanced with increasing USP duration. This leads to a gradual increase in the surface hardness of the material, until a maximum value is reached.

3.4 Surface roughness

2D and 3D surface topographies of UT sample and T1–T5 samples are shown in Fig. 5. The surfaces of the USP-treated samples have unevenly distributed pits with different sizes, compared to UT sample. These pits generated by USP treatment represent the root cause of the increase in the material’s roughness. As can be seen in Fig.5, there are almost no portions of surface that have not been impacted by the shot peening particles. According to the SAEJ2277 standard, this indicates that the shot peening coverage is 100%. The rest of the samples are exposed to USP durations of >50 s, so it is inferred that all of USP-treated samples have at least 100% shot peening coverage.

The variations in roughness parameters (R_a , R_q , and R_t) with the increase in treatment duration of UT and T1–T5 samples are shown in Fig. 6, where it can be seen that the surface

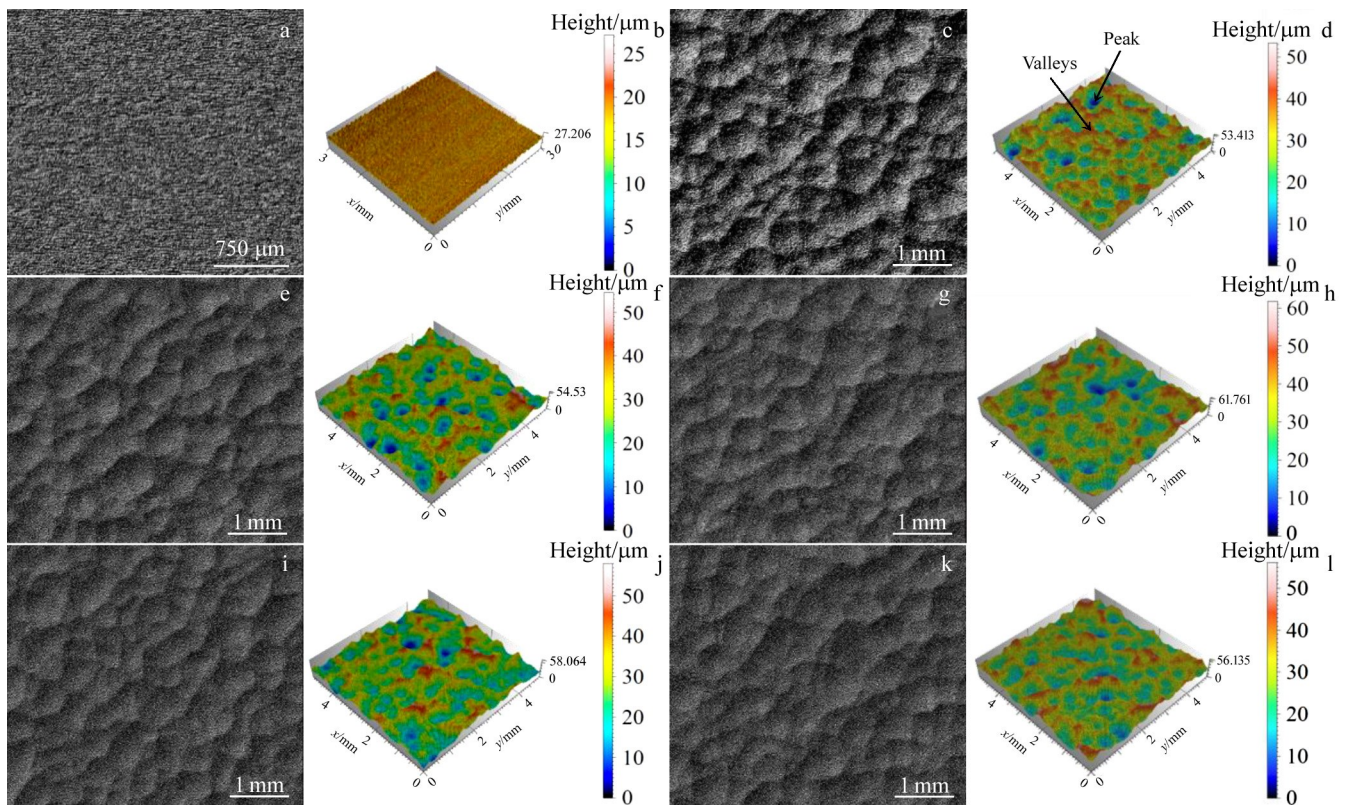


Fig.5 2D and 3D surface topographies of different samples: (a–b) UT, (c–d) T1, (e–f) T2, (g–h) T3, (i–j) T4, and (k–l) T5

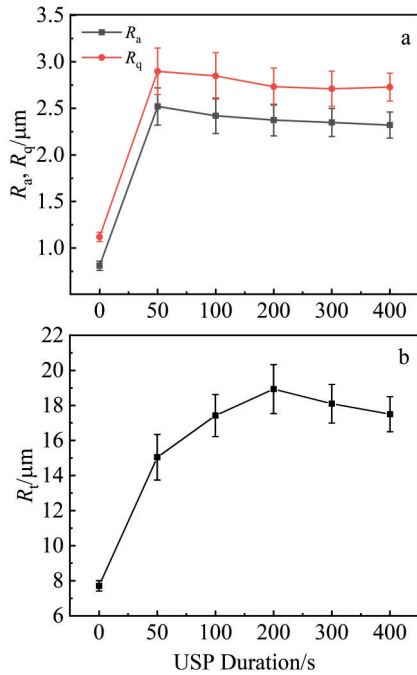


Fig.6 Effect of USP duration on surface roughness: (a) R_a and R_q ; (b) R_i

roughness of the samples increase rapidly after USP treatment for 50 s. R_a increases from its original value of 0.81 μm to 2.52 μm , with a rise of 211.1%. As USP duration increases, R_a shows a slightly decreasing tendency before stabilizing. After USP treatment for 50 s, R_i increases rapidly from its original value of 7.71 μm to 15.04 μm . With the further increase in USP duration, R_i gradually increases until it reaches a maximum value of 18.93 μm at 200 s. After that, R_i gradually decreases with the increase in USP duration until finally stabilizing.

3.5 Static contact angle

The measured static contact angles of the sample surfaces are shown in Fig. 7. The untreated samples have a minimum static contact angle of 73.75°, while the treated samples all have higher values, indicating that the material's surface has a lower wettability after being treated by USP. At first, the static contact angle increases with the increase in USP duration, until it reaches a maximum value at 200 s. Thereafter, it decreases slowly. The variation of static contact angle depends on surface free energy and roughness of material^[30]. The surface roughness of the material increases following USP treatment, and this roughened surface helps it to resist the contact with corrosive substances. After USP treatment, the stability of the passivation film on the material's surface also increases, which adjusts its surface free energy and gives it a lower wettability.

3.6 Cycling corrosion rate of salt spray

The corrosion rates, post-corrosion surface morphologies, and depths of corrosion pits in UT and T1–T5 samples are obtained to study the effect of USP duration on the corrosion-

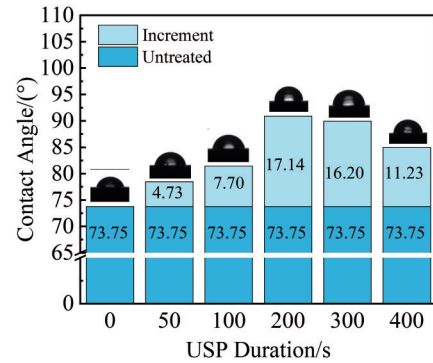


Fig.7 Effect of USP duration on static contact angles of different samples

related properties of the material. The corrosion rate for each sample is shown in Fig.8, which was calculated using Eq. (1). The corrosion rate of the untreated sample is 0.068 $\text{mm}\cdot\text{a}^{-1}$, and that of the treated samples shows generally decreasing trend following different durations of USP treatment. As USP duration increases, the corresponding corrosion rates are 0.078, 0.072, 0.073, 0.048, and 0.040 $\text{mm}\cdot\text{a}^{-1}$. The sample treated for 400 s has the lowest corrosion rate, which is 41.2% lower than that of the untreated sample. By contrast, the corrosion rates of T1, T2, and T3 samples are all higher than that of UT sample. The surface morphologies of the samples after cyclic salt spray corrosion test are shown in Fig.9. The maximum depth values and the average depth values of each sample in the ten surface corrosion pits are shown in Fig.10 and Fig.11, respectively. The number, size, and depth of the corrosion pits in a material can reflect its degree of corrosion. The degree of corrosion in UT sample is higher, as there are more corrosion pits with deeper depth. The sample treated for 400 s shows the lightest degree of corrosion, because of the lowest number of corrosion pits on the surface and the shallowest average depth of corrosion pit. This demonstrates that appropriate USP parameters can effectively improve the corrosion resistance of this material, and reduce the occurrence of pitting corrosion. Conversely, improper parameters can lower its corrosion resistance and promote the occurrence of pitting corrosion.

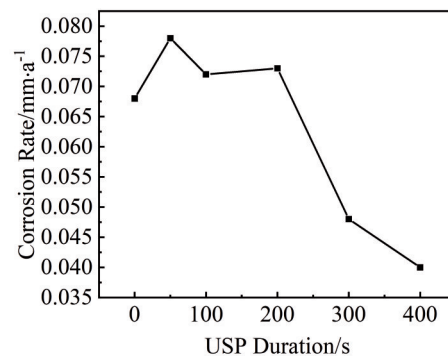


Fig.8 Effect of USP duration on corrosion rate

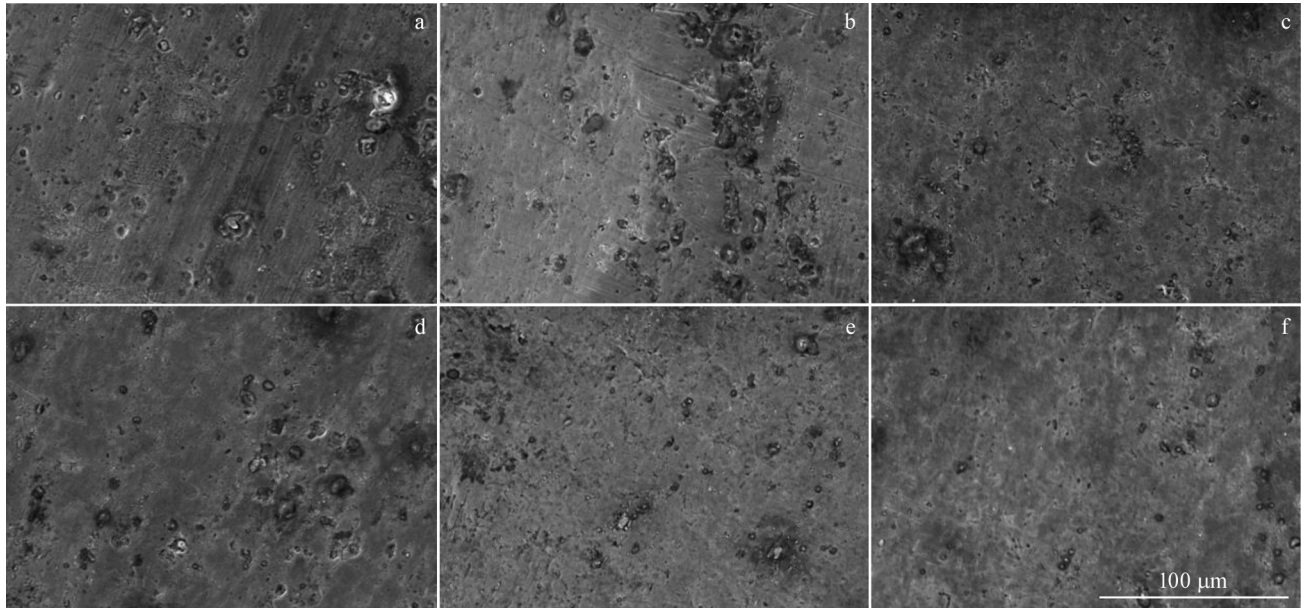


Fig.9 Surface morphologies after cyclic salt spray corrosion of different samples: (a) UT, (b) T1, (c) T2, (d) T3, (e) T4, and (f) T5

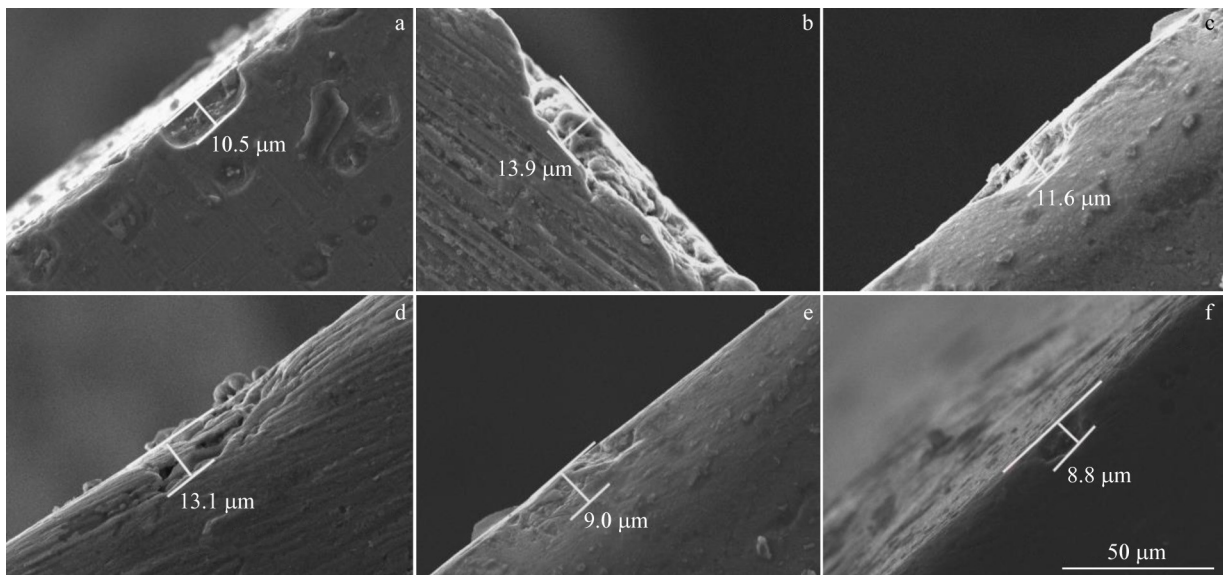


Fig.10 Maximum value of surface corrosion pit depth after cyclic salt spray corrosion of different samples: (a) UT, (b) T1, (c) T2, (d) T3, (e) T4, and (f) T5

4 Discussion

4.1 Corrosion mechanism

CCT simulates the corrosion process of the material in a marine environment. Chloride ions in the environment leaching into the material represents the main mechanism underlying the formation of pitting corrosion. Fig. 12 shows the surface morphologies and EDS spectra of T1 sample before and after corrosion, showing that the compositional changes on the surface of the alloy mainly comprise: (1) a decrease in aluminum percentage of the alloys' mass; (2) an increase in mass percentage of oxygen. Incorporated the corrosion process of the material in a simulated marine

environment, aluminum is in the active position in the anode region, promoting a loss of electrons that generates aluminum ions. Under the action of the corrosive electrolyte, oxygen gas in the cathode region is prone to undergo the oxygen uptake reaction, generating hydroxide ions. The full corrosion mechanism is shown in Fig. 13. The anodic reaction is shown in Eq.(3):



while the cathodic reaction takes the form as follows:



Aluminum ions generated in the anodic region combines with hydroxide ions generated in the cathodic region to form aluminum hydroxide. On the one hand, aluminum oxide is

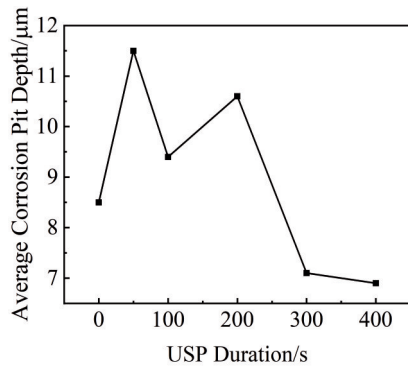
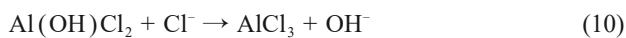
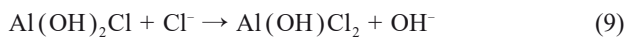
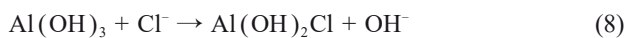


Fig.11 Average value of surface corrosion pit depth after cyclic salt spray corrosion

generated as a result of the dehydration of aluminum hydroxide. On the other hand, chloride ions in the marine environment exerts strong adsorption and erosion effects, gradually replacing the hydroxide ions in aluminum hydroxide through competitive adsorption. A series of reactions take place, eventually generating water-soluble aluminum chloride, via the following steps:



Water-soluble aluminum chloride is therefore washed away in a marine environment. The finally generated corrosion product is aluminum oxide. The corrosion resistance of aluminum can be improved in the following ways: (1) protecting the material from attack by chloride ions; (2) improving the stability of the passivation film on the metal's surface and slowing down the aluminum dissolution

reaction at the anode; (3) reducing the metal surface area that comes into contact with the corrosive medium.

4.2 Mechanism for strengthening corrosion resistance by USP

According to the results, the corrosion resistance of 6061-T6 aluminum alloy is significantly improved after USP treatment with appropriate parameters. According to the experiments and analysis of the mechanism behind aluminum corrosion, there are four main factors about the effect of USP on the corrosion resistance of 6061-T6 aluminum. (1) USP treatment strengthens the surface layer of the material to produce intense plastic deformation, generating a large number of dislocations and twins within the material that distort its lattice. The macroscopic manifestation of this process on the material's surface introduces residual compressive stress. Lai et al^[31] showed that the residual compressive stress in 304 stainless steels increased with the increase in USP duration over a certain range, and the residual compressive stress layer was deepened. Other studies have shown that increasing the residual compressive stress in a material can reduce the electrochemical activity of its surface metal atoms and decrease the density of its passivation current^[32-33]. This also slows down the dissolution reaction that occurs at the aluminum anode. (2) After USP treatment, the surface layer of the material may prevent the diffusion of chloride ions, owing to grain refinement and an increase in grain boundaries. The fine grain-strengthening effect and the work-hardening effect improve the surface hardness of the material, which makes the passivation film produced on the material's surface more uniform, thus providing better erosion resistance to chloride ions. (3) The surface roughness parameters (R_a , R_q , and R_l) are changed to varying degrees by USP treatment. A higher roughness means a larger contact area between the material's surface and the corrosive medium, making it easier for corrosive substances to

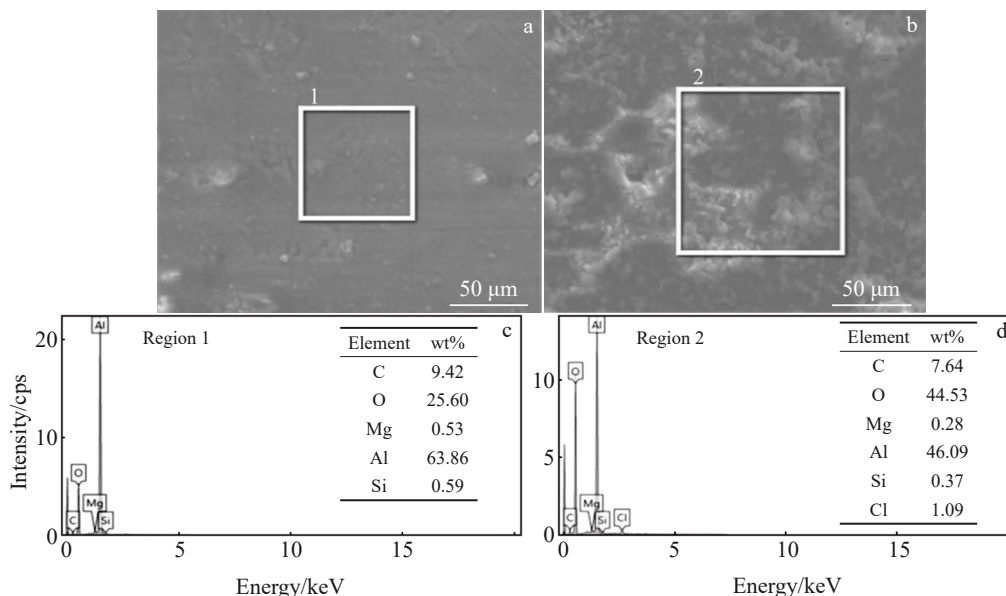


Fig.12 Surface morphologies (a-b) and EDS results (c-d) of T1 sample before (a, c) and after (b, d) corrosion testing

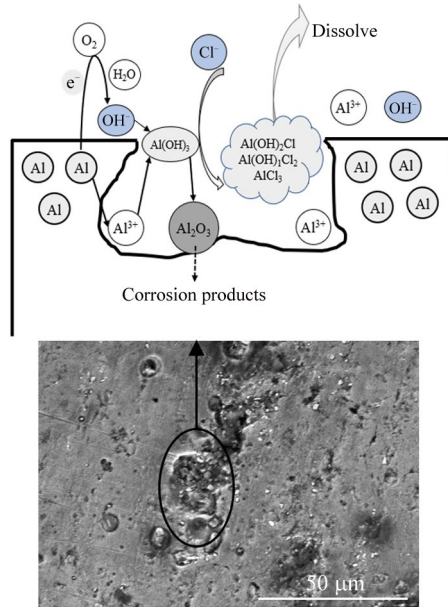


Fig.13 Corrosion mechanism diagram of 6061-T6 aluminum alloy

be deposited. These factors reduce the corrosion resistance of the material. Consistent with the results of Shao et al^[34], magnesium alloys with lower surface roughness show higher corrosion resistance. (4) The wettability of material decreases after USP treatment, which reduces the contact area between material and the corrosive medium, thus slowing the corrosion rate.

Fig. 14 presents a model depicting the surface corrosion mechanism for USP-treated materials. The effect of USP duration on the corrosion resistance of the material can be analyzed according to this model. The strengthening layers produced on the material surface through compressive residual stress, grain refinement, increased grain boundaries, increased hardness, and increased static contact angle all strengthen its corrosion resistance. Increasing the material surface roughness parameters (R_a , R_q , and R_t) weakens corrosion resistance. The change in the corrosion resistance of the material after USP treatment results from a competitive mechanism between the

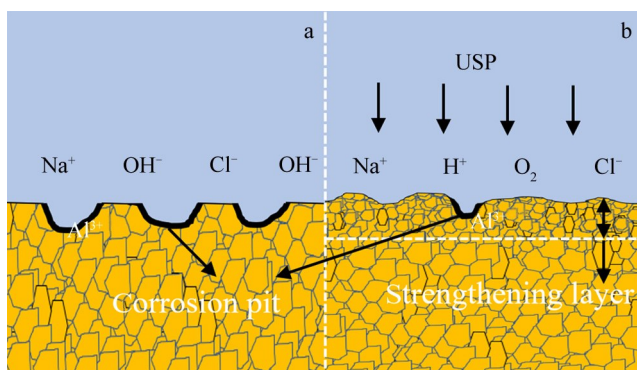


Fig.14 Surface corrosion mechanisms of UT sample (a) and USP-treated sample (b)

strengthening and weakening terms. Comparing UT, T1, T2, and T3, it can be seen that the thickness of the strengthening layer on the material surface is thinner when USP duration is shorter. However, the roughness parameters (R_a , R_q , and R_t) are increased compared to the untreated sample. The weakening term therefore plays a more dominant role in the overall corrosion equation at this duration. As the USP duration continues to increase, the thickness of the strengthening layer on the material's surface increases further. At the same duration, the total height of the profile (R_t) begins to decrease. At this point, the strengthening term plays a dominant role, the detrimental effect of the weakening term is reduced, and the corrosion behavior of the treated material becomes apparent. According to this analysis, the corrosion resistance of the material shows an increasing trend, followed by a decreasing one, as USP duration increases. Based on the experimental results, it can be predicted that a material treated with a long duration of USP has the peaks on its polished surface, yielding a thicker reinforcing layer with low roughness, ultimately resulting in a significant improvement to corrosion resistance.

5 Conclusions

1) The degree of grain refinement, the number of grain boundaries, and the hardness of the surface layer of 6061-T6 aluminum alloy increase with increasing durations of USP treatment. The total height of contour (R_t) and the static contact angle first increase, then decrease with the increase in USP duration, and the change in corrosion rate shows a similar trend.

2) USP treatment increases the corrosion resistance of the material by increasing the values of its strengthening terms. The introduction of compressive residual stress, grain refinement, increased grain boundaries, higher static contact angles, and improved hardness all increase the material's corrosion resistance. Conversely, USP also influences the material's weakening terms, including surface roughness, which also increases under USP treatment. The final change in the material's corrosion resistance is the result of relative changes in the strengthening terms relative to those in the weakening terms, through a competitive mechanism. When the strengthening terms are dominated, the corrosion resistance of USP-treated sample will increase. Conversely, when the weakening terms are dominated, corrosion resistance will decrease.

3) When 6061-T6 aluminum alloy is treated with USP for 400 s, the thickness of the reinforced layer on the surface is maximum and the surface roughness decreases compared to that of the sample treated for 200 s, and its corrosion rate reaches the lowest value of $0.040 \text{ mm} \cdot \text{a}^{-1}$. The corrosion rate is reduced by 41.2% compared to that of the untreated sample. It also shows the best results in terms of the lowest number of surface corrosion pits with the shallowest depth.

References

- 1 Yuan Z Y, Wang Y B, Zou R et al. *Rare Metal Materials and Engineering*[J], 2022, 51(5): 1589
- 2 Xi R, Xie J, Yan J B. *Construction and Building Materials*[J], 2024, 411: 134520
- 3 Starke E A, Staley J T. *Progress in Aerospace Sciences*[J], 1996, 32(2): 131
- 4 Li M C, Seyeux A, Wiame F et al. *Corrosion Science*[J], 2020, 176: 109040
- 5 Mondou E, Proietti A, Charvillat C et al. *Corrosion Science*[J], 2023, 221: 111338
- 6 Xiong Y D, Robson J D, Cao Z J et al. *Corrosion Science*[J], 2023, 225: 111570
- 7 Peng C, Cao G W, Gu T Z et al. *Corrosion Science*[J], 2023, 210: 110840
- 8 Sun Q Q, Cao F H, Wang S. *Corrosion Science*[J], 2022, 195: 110021
- 9 Karthik D, Deshmukh K, Praveenkumar K et al. *Optics & Laser Technology*[J], 2024, 172: 110537
- 10 Zhang Z H, Fu X S, Cao Z W et al. *Optics & Laser Technology*[J], 2024, 174: 110643
- 11 Wang Z D, Sun G F, Lu Y et al. *Surface and Coatings Technology*[J], 2020, 385: 125403
- 12 Zhu L H, Guan Y J, Wang Y J et al. *Surface and Coatings Technology*[J], 2017, 317: 38
- 13 Chen Y, Du J, Deng S et al. *Journal of Alloys and Compounds*[J], 2023, 934: 168023
- 14 Han M X, Du J, Chen Y et al. *Journal of Alloys and Compounds*[J], 2024, 980: 173633
- 15 Liu H, Chen J B, Wang S et al. *Corrosion Communications*[J], 2023, 10: 48
- 16 Sun Q Q, Han Q Y, Wang S et al. *Surface and Coatings Technology*[J], 2020, 398: 126127
- 17 Kumar P, Mahobia G S, Singh V et al. *International Journal of Fatigue*[J], 2023, 166: 107289
- 18 Xu S, Cao Y, Duan B B et al. *Surface and Coatings Technology*[J], 2023, 458: 129325
- 19 Qin Z, Li B, Chen T Y et al. *International Journal of Fatigue*[J], 2023, 175: 107799
- 20 Zhang Q, Li S F, Cao Y et al. *Journal of Alloys and Compounds*[J], 2023, 948: 169704
- 21 Ganguly S, Chaubey A K, Gope R et al. *Journal of Alloys and Compounds*[J], 2023, 966: 171203
- 22 Kumar S, Chattopadhyay K, Singh V. *Materials Characterization*[J], 2016, 121: 23
- 23 Ma Y Q, Li K P, Li C L et al. *Journal of Power Sources*[J], 2024, 594: 233999
- 24 Lu S H, Wang Q C, Zhang Y et al. *Journal of Materials Science & Technology*[J], 2023, 152: 94
- 25 Li Y J, Liu X T, Wang F et al. *Materials Chemistry and Physics*[J], 2024, 313: 128720
- 26 Zhang X H, Liu J, Xia M et al. *International Journal of Machine Tools and Manufacture*[J], 2023, 185: 103993
- 27 Efe Y, Karademir I, Husem F et al. *Applied Surface Science*[J], 2020, 528: 146922
- 28 Figueiredo R B, Kawasaki M, Langdon T G. *Progress in Materials Science*[J], 2023, 137: 101131
- 29 Yin F, Han P C, Han Q Y et al. *Materials & Design*[J], 2024, 239: 112786
- 30 Tong Z P, Zhang Y Z, Chen J et al. *Surface and Coatings Technology*[J], 2023, 472: 129945
- 31 Lai H H, Cheng H C, Lee C Y et al. *Journal of Materials Processing Technology*[J], 2020, 284: 116747
- 32 Trdan U, Grum J. *Corrosion Science*[J], 2012, 59: 324
- 33 Luo K Y, Xing Y, Sun M R et al. *Corrosion Science*[J], 2024, 228: 111794
- 34 Shao Z X, Li P B, Zhang C et al. *Journal of Magnesium and Alloys*[J], 2024, 12(6): 2520

超声喷丸对 6061-T6 铝合金表面完整性及抗腐蚀性能的影响

李 坤, 温腾飞, 李少龙, 王 成
(安徽理工大学 机电工程学院, 安徽 淮南 232001)

摘 要: 通过表面形貌、显微硬度、X射线衍射及静态接触角等实验研究了超声喷丸 (USP) 对 6061-T6 铝合金的表面完整性及抗腐蚀性能的变化。结果表明, USP 后材料表面晶粒尺寸减小了 43%, 残余压应力有增大趋势, 粗糙度与硬度分别增加了约 211.1% 和 35%, 静态接触角先增大再略微降低。采取称重、扫描电镜及能谱分析等手段对循环盐雾加速腐蚀实验后的试样进行了研究。结果显示, USP 可以将腐蚀速率降低 41.2%。建立了 USP 材料表面腐蚀机理模型, 讨论了 USP 提高材料抗腐蚀性能的机理, 引入残余应力、晶粒细化、晶界增多、硬度增加以及静态接触角增大是材料抗腐蚀性能提升的主要因素, 粗糙度增加则弱化了表面的抗腐蚀性能。

关键词: 6061-T6 铝合金; 抗腐蚀性能; 表面完整性; 超声喷丸

作者简介: 李 坤, 男, 1978 年生, 博士, 副教授, 安徽理工大学机电工程学院, 安徽 淮南 232001, E-mail: kli@aust.edu.cn